Disproportionation Pathways of Aqueous Hyponitrite Radicals ($HN_2O_2^{\bullet}/N_2O_2^{\bullet-}$)

Gregory A. Poskrebyshev,[†] Vladimir Shafirovich,[‡] and Sergei V. Lymar*[,†]

Chemistry Department, Brookhaven National Laboratory, Upton, New York 11973, and Chemistry Department and Radiation and Solid State Laboratory, New York University, New York, New York 10003

Received: April 14, 2008; Revised Manuscript Received: July 2, 2008

Pulse radiolysis and flash photolysis are used to generate the hyponitrite radicals ($HN_2O_2^{\bullet}/N_2O_2^{\bullet-}$) by one-electron oxidation of the hyponitrite in aqueous solution. Although the radical decay conforms to simple second-order kinetics, its mechanism is complex, comprising a short chain of NO release−consumption steps. In the first, rate-determining step, two $N_2O_2^{\bullet-}$ radicals disproportionate with the rate constant $2k = (8.2 \pm 0.5) \times 10^7$ M^{-1} s^{-1} (at zero ionic strength) effectively in a redox reaction regenerating $N_2O_2^{2-}$ and releasing two NO. This occurs either by electron transfer or, more likely, through radical recombination−dissociation. Each NO so-produced rapidly adds to another $N_2O_2^{\bullet-}$, yielding the $N_3O_3^-$ ion, which slowly decomposes at 300 s^{-1} to the final $N_2O + NO_2^-$ products. The $N_2O_2^{\bullet-}$ radical protonates with $pK_a = 5.6 \pm 0.3$. The neutral $HN_2O_2^{\bullet}$ radical decays by an analogous mechanism but much more rapidly with the apparent second-order rate constant $2k = (1.1 \pm 0.1) \times 10^9$ M^{-1} s^{-1}. The $N_2O_2^{\bullet-}$ radical shows surprisingly low reactivity toward O_2 and $O_2^{\bullet-}$, with the corresponding rate constants below 1×10^6 and 5×10^7 M^{-1} s^{-1}. The previously reported rapid dissociation of $N_2O_2^{\bullet-}$ into N_2O and $O^{\bullet-}$ does not occur. The thermochemistry of $HN_2O_2^{\bullet}/N_2O_2^{\bullet-}$ is discussed in the context of these new kinetic and mechanistic results.

Introduction

The hyponitrite radical anion ($N_2O_2^{\bullet-}$) and its conjugate acid ($HN_2O_2^{\bullet}$) can be obtained in aqueous solution either by one-electron oxidation of hyponitrite ($N_2O_2^{2-}$; hence, the radical name)[1] or by one-electron reduction of nitric oxide[2−4] (Figure 1). In the latter case, the precursor can be either nitroxyl (^{1}HNO, singlet ground state) or nitroxyl anion ($^3NO^-$, triplet ground state). Spin prohibition in their acid−base equilibration gives rise to two independent pathways leading to $HN_2O_2^{\bullet}/N_2O_2^{\bullet-}$; although NO is added in both pathways, the rates differ dramatically.[4−7] It is due to these complications that considerable confusion has persisted in the literature for over three decades concerning the fundamental properties of the aqueous hyponitrite radical derived from pulse radiolysis experiments involving reduction of NO. Recently, we have suggested a major revision that includes the radical absorption spectra, acidity, redox properties, and stability with respect to dissociation back into nitric oxide and nitroxyl.[1]

The hyponitrite radicals are also known in the gas phase[8,9] and in solid argon and neon.[10−13] Although both *cis*-[ON═NO]$^{\bullet-}$ and *trans*-[ON═NO]$^{\bullet-}$ have been generated from various precursors and stabilized toward spontaneous isomerization in the cryogenic inert-gas matrixes, theory predicts lower energy for the trans isomers of both $HN_2O_2^{\bullet}$ and $N_2O_2^{\bullet-}$.[1,14−17] Considering these results, it is reasonable to assume that the radicals prepared by the one-electron oxidation of hyponitrite, which has a trans configuration, will retain the parent's trans structure, as shown in Figure 1.

Lying between NO and N_2O in terms of the nitrogen oxidation state, the hyponitrite radical is a potentially important species in the redox transformations of nitrogen in biological (nitrification/denitrification, assimilatory nitrite reduction) and aquatic environmental processes. We have estimated that $HN_2O_2^{\bullet}/N_2O_2^{\bullet-}$ are both strongly oxidizing and moderately reducing, which engenders the expectation of rich chemistry. At the same time, the reactivity of these radicals remains largely unexplored. In this work, we use pulse radiolysis and flash photolysis to generate the hyponitrite radicals and investigate their decay mechanism, which occurs through a surprisingly complex redox disproportionation.

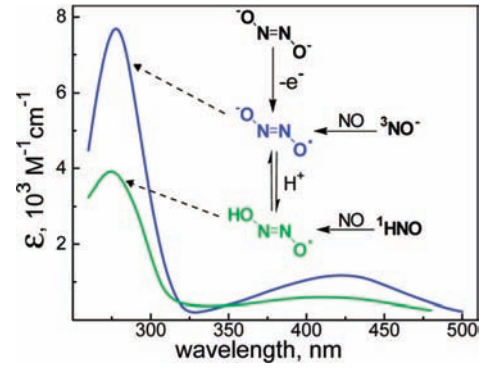

Figure 1. Formation pathways and absorption spectra of the hyponitrite radicals.[1,4]

Experimental Section

Sample Solutions. Analytical-grade buffers, $HClO_4$, and NaOH and Milli-Q purified (ASTM type I) water were used throughout. Sodium *trans*-hyponitrite ($Na_2N_2O_2 \cdot xH_2O$ from Aldrich, $x = 3.0 \pm 0.2$)[1] was used as received. Its alkaline (pH 12−13) or acidic (pH 2−3) stock solutions were prepared daily and kept on ice. The hyponitrite concentrations were assayed spectrophotometrically at the 248 nm absorption maximum of $N_2O_2^{2-}$ using $\varepsilon_{248} = 6550$ M^{-1} cm^{-1}.[18] An aliquot of the stock was diluted to the desired pH, saturated with N_2O or its mixtures with NO or O_2 (as described in detail elsewhere[4]), and used for pulse radiolysis experiments within 1 h.

* To whom correspondence should be addressed. Tel: 631-344-4333. Fax: 631-344-5815. E-mail: lymar@bnl.gov.
† Brookhaven National Laboratory.
‡ New York University.

10.1021/jp803230c CCC: $40.75
Published on Web 08/15/2008

Kinetic Measurements. The pulse radiolysis was carried out with 2 MeV electrons from a Van de Graaff accelerator; pulse widths were in the range of 0.06−0.8 μs. Either one or three passes of analyzing light through a 2 cm long quartz cell were used in the detection optical path. For the kinetics recorded on a time scale of less than 100 μs, the analyzing Xe-arc light source was pulsed. All experiments were done with temperature stabilization at 25 ± 0.5 °C. The radiation yields of radicals (here and throughout in a number of radicals per 100 eV of absorbed energy) were taken as $G(OH^{\bullet}) = 6.1$ and $G(H^{\bullet}) = 0.6$ in N_2O-saturated solutions, $G(OH^{\bullet}) = 2.8$ and $G(O_2^{\bullet-}) = 3.4$ in O_2-saturated solutions, and $G(OH^{\bullet}) = 6.0$ and $G(O_2^{\bullet-}) = 0.6$ in solution saturated with a 9:1 or 4:1 N_2O to O_2 gaseous mixture. Dosimetry was performed with a N_2O-saturated 10 mM KSCN solution using $G\varepsilon = 4.87 \times 10^4$ ions (100 eV)$^{-1}$ M^{-1} cm^{-1} for the $(SCN)_2^{\bullet-}$ radical at 472 nm. Continuous gamma irradiation was performed in a well-type Co-60 source with about 2 s accuracy of exposure at a 110 Gy/min dose rate. Kinetic modeling was carried out with the INTKIN software developed at the Brookhaven National Laboratory by H. A. Schwarz.[19]

Flash photolysis was done under O_2 saturation in a flow cell, as described elsewhere.[5−7] An alkaline solution of $N_2O_2^{2-}$ was mixed with buffer also containing $S_2O_8^{2-}$ prior to entering the cell. A 308 nm excimer laser was employed to cleave $S_2O_8^{2-}$ into a pair of $SO_4^{\bullet-}$ radicals, which then were used to oxidize hyponitrite.

Results

Decay Kinetics. Previously, we have shown that all primary radicals from water radiolysis ($OH^{\bullet}$, e_{aq}^-, and $H^{\bullet}$) can be employed to generate the hyponitrite radical in a N_2O-saturated solution of hyponitrite under both alkaline and acidic conditions.[1] Omitting rapid reactions converting e_{aq}^- and $H^{\bullet}$ into $OH^{\bullet}$,[20] the principal reactions producing the hyponitrite radicals were

$$N_2O_2^{2-} + OH^{\bullet} \rightarrow N_2O_2^{\bullet-} + OH^- \qquad k_1 = 8.8 \times 10^9\ M^{-1}\ s^{-1} \quad (1)$$

$$HN_2O_2^- + OH^{\bullet} \rightarrow N_2O_2^{\bullet-} + H_2O \qquad k_2 = 4.2 \times 10^9\ M^{-1}\ s^{-1} \quad (2)$$

$$H_2N_2O_2 + OH^{\bullet} \rightarrow HN_2O_2^{\bullet} + H_2O \qquad k_3 = 4 \times 10^7\ M^{-1}\ s^{-1} \quad (3)$$

with their relative contribution governed by the acid dissociation constants $pK_a(H_2N_2O_2) = 7.2$ and $pK_a(HN_2O_2^-) = 11.5$.[21] We also observed a characteristic UV absorption spectrum of the hyponitrite radical (Figure 1) and interpreted its changes with pH as the evidence for the acid−base equilibrium

$$HN_2O_2^{\bullet} \rightleftarrows H^+ + N_2O_2^{\bullet-} \quad (4)$$

for which a pK_4 of 5.5 was obtained.[1] Both $N_2O_2^{\bullet-}$ and $HN_2O_2^{\bullet}$ exhibit maxima in the near-UV region (Figure 1), and their decay is best observed around 290 nm, where interference from both the absorption and bleaching of the starting material is negligible.

As shown in Figure 2, the decay in acidic solution occurs monotonically at all wavelengths and is much more rapid than the decay in alkaline solution, where the appearance of a long-lived intermediate is observed at around 380 nm concurrent with the $N_2O_2^{\bullet-}$ decay. The decay traces at 290 nm can be very well fitted to second-order kinetics

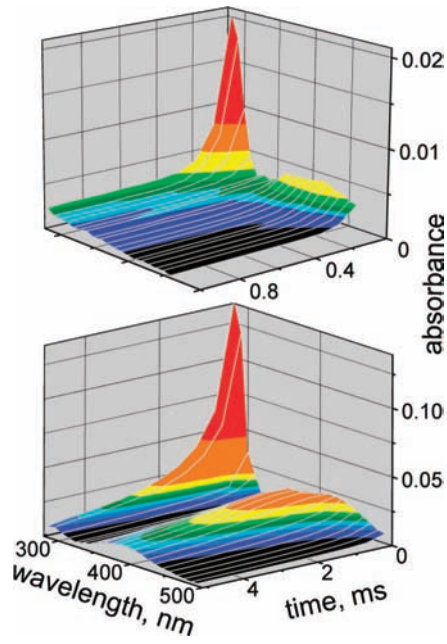

Figure 2. Spectral changes during the hyponitrite radical decay in acidic (pH 3, top) and alkaline (pH 12, bottom) solutions. Note the difference in time scales and the appearance of species absorbing near 380 nm in alkali.

$$A_t = \frac{A_0 - A_f}{1 + 2k_{app}[R]_0 \times t} + A_f \quad (5)$$

in both acid and alkali (Figure 3), where A_0 and A_f are the initial and final absorbances, respectively, and the third fitting parameter $2k_{app}[R]_0$ yields the apparent second-order rate constant, k_{app}, if the initial concentration of radicals can be evaluated from A_0 and the light path l, that is, $[R]_0 = A_0/\varepsilon_{290}l$. Using the values of molar absorptivities $\varepsilon_{290}(N_2O_2^{\bullet-}) = 5900 \pm 300$ and $\varepsilon_{290}(HN_2O_2^{\bullet}) = 3100 \pm 300$ M^{-1} cm^{-1} measured in the previous work[1] and varying the radiation dose, we have obtained a good linearity of $2k_{app}[R]_0$ with $[R]_0$ (Figure 3), from which $2k_{app} = (5.4 \pm 0.3) \times 10^8$ M^{-1} s^{-1} for the $N_2O_2^{\bullet-}$ radical at a 1 M ionic strength and $2k_{app} = (2.2 \pm 0.2) \times 10^9$ M^{-1} s^{-1} for the $HN_2O_2^{\bullet}$ radical, with most of the error coming from the uncertainties in molar absorptivities. It would thus appear that the radicals decay through simple recombination reactions

$$N_2O_2^{\bullet-} + N_2O_2^{\bullet-} \rightarrow \text{products} \quad (6)$$

$$HN_2O_2^{\bullet} + HN_2O_2^{\bullet} \rightarrow \text{products} \quad (7)$$

This formulation is supported by the observed independence of $2k_{app}$ on the ionic strength in acidic media and by the Debye−Hückel dependence corresponding to a reaction between the two singly charged species in alkali (Figure 4, inset).

The second-order decay fits remain good throughout the pH region from 2.5 to 12, and the pH dependence of the $2k_{app}/\varepsilon_{app}$ value is shown in Figure 4. Its titration curve appearance is in accord with the equilibrium in reaction 4. Introducing, for generality, a cross-recombination reaction

$$N_2O_2^{\bullet-} + HN_2O_2^{\bullet} \rightarrow \text{products} \quad (8)$$

we obtain for the pH dependence

$$\frac{2k_{app}}{\varepsilon_{app}} = \frac{2k_6K_4^2 + 2k_7[H^+]^2 + 2k_8K_4[H^+]}{\{\varepsilon(N_2O_2^{\bullet-})K_4 + \varepsilon(HN_2O_2^{\bullet})[H^+]\}(K_4 + [H^+])} \quad (9)$$

The molar absorptivities are known (Figure 1) and the magnitudes of k_6 and k_7 are set by the plateau regions, leaving K_4 and k_8 as the only fitting parameters, and the fit with $pK_4 = 5.6$ and $k_8 = 5 \times 10^8$ M^{-1} s^{-1} is shown in Figure 4. Within its estimated uncertainty of ±0.3, this pK_4 value is the same as that determined previously from the absorption spectra.[1] Because k_7 is so much larger than k_6, the fit is extremely insensitive to k_8 as long as it is kept below k_7, but k_8 can be decreased to zero without critically spoiling the fit. It is however reasonable that k_8 should lie somewhere between k_6 and k_7.

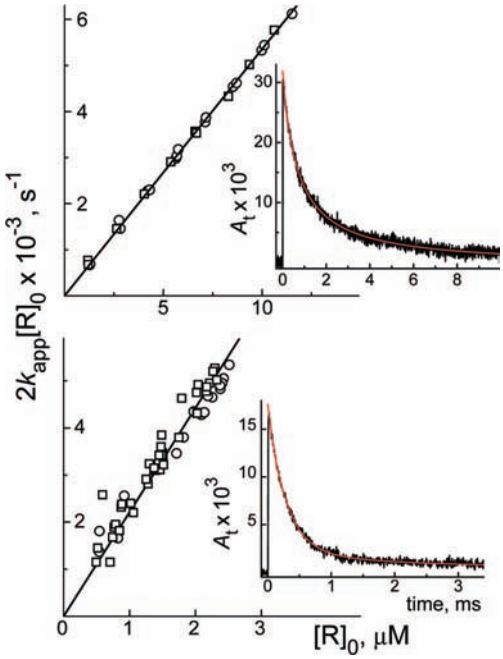

Figure 3. Observed rate constants, k_{app}, for the hyponitrite radical decay obtained by fitting the transient absorptions at 290 nm, A_t, to the second-order rate law in eq 5. Upper panel: alkaline solution containing 10 mM NaOH and 1.64 (○) or 3.9 mM (□) $Na_2N_2O_2$ at a 1 M ionic strength ($NaClO_4$). Lower panel: acidic solution at pH 2.7−3.3 adjusted with $HClO_4$ and containing 0.5 (○) or 1 mM (□) of $Na_2N_2O_2$. The straight lines give the linear fits corresponding to the bimolecular rate constants $2k_{app} = 5.4 \times 10^8$ M^{-1} s^{-1} (upper) and 2.2×10^9 M^{-1} s^{-1} (lower). The insets show typical transient absorption decay kinetics and their second-order fits (red lines) under both alkaline and acidic conditions.

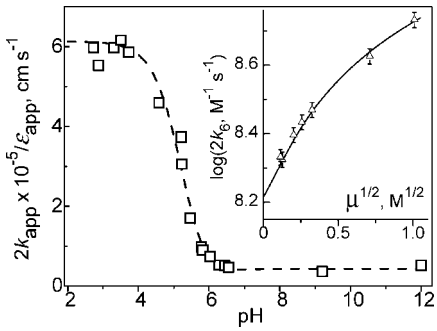

Figure 4. Dependence upon pH of the observed rate constant for the decay of the hyponitrite radical through reactions 6−8. The values of $2k_{app}/\varepsilon_{app}$ were obtained by fitting the transient absorptions to the second-order rate law in eq 5. The dashed curve corresponds to eq 9 (see text for equation parameters that were used). Inset shows the ionic strength, μ, dependence of k_6 in the alkaline region (pH > 9) and its Debye−Hückel fit (line): $\log 2k_6 = \log 2k_6(\mu \rightarrow 0) + 1.02\ \mu^{1/2}/(1 + \mu^{1/2})$, with the limiting value $2k_6(\mu \rightarrow 0) = (1.64 \pm 0.10) \times 10^8$ M^{-1} s^{-1}.

SCHEME 1: Alternative Recombination Mechanisms Yielding the Stoichiometry of Reaction 12[a]

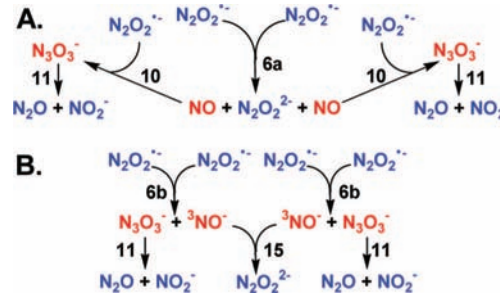

[a] Initial and final species are in blue, and intermediates are in red.

Although we have so far treated the hyponitrite radical decay in terms of simple recombination reactions, it will become clear in the following section that the apparent bimolecular rate constants determined from the data in Figures 3 and 4, while related to reactions 6−8, are not their actual rate constants.

Intermediates and Mechanism. As seen in Figure 2 for the alkaline solution, an intermediate whose absorption rises concurrently with $N_2O_2^{\bullet-}$ decay, peaks and then decays is observed between 330 and 420 nm. We will now show that this intermediate can be identified as the $N_3O_3^-$ anion, and its formation and decay can be described by the following mechanism

$$N_2O_2^{\bullet-} + N_2O_2^{\bullet-} \rightarrow N_2O_2^{2-} + 2NO \qquad \text{rate-limiting} \quad (6a)$$

$$N_2O_2^{\bullet-} + NO \rightarrow N_3O_3^- \qquad \text{rapid} \quad (10)$$

$$N_3O_3^- \rightarrow N_2O + NO_2^- \qquad \text{slow} \quad (11)$$

where reaction 6a is rate-limiting for the formation of $N_3O_3^-$. This mechanism, depicted in Scheme 1A, effectively amounts to redox disproportionation of the $N_2O_2^{\bullet-}$ radical. Beginning with $OH^{\bullet}$, the overall stoichiometry is

$$4OH^{\bullet} + 3N_2O_2^{2-} \rightarrow 4OH^- + 2NO_2^- + 2N_2O \quad (12)$$

From the decay of $N_2O_2^{2-}$ absorption in a N_2O-saturated solution under continuous radiolysis with a Co-60 gamma source, we have obtained ~0.7 for the ratio of $N_2O_2^{2-}$ consumption to $OH^{\bullet}$ production rates (Supporting Information Figure S1), which is close to the 3/4 ratio prescribed by the stoichiometry in reaction 12.

Previously, the $N_3O_3^-$ anion has been observed in the pulse radiolysis of aqueous NO solutions,[2−4] where the anion is produced as a result of NO reduction by the hydrated electron followed by concatenation of two more NO radicals, that is, the reaction sequence

$$e_{aq}^- + 3NO \rightarrow {}^3NO^- + 2NO \rightarrow N_2O_2^{\bullet-} + NO \rightarrow N_3O_3^- \quad (13)$$

The absorption spectrum of the so-created "authentic" $N_3O_3^-$ anion with its distinct peak at 380 nm is reproduced as a line in Figure 5. At sufficient concentration of NO, reaction sequence 13 is complete on a microsecond time scale, following which the $N_3O_3^-$ anion decays exponentially through reaction 11 with a characteristic time of 3.3 ms in neutral solutions.[3,4] As with the "authentic" $N_3O_3^-$, the intermediate in the recombination

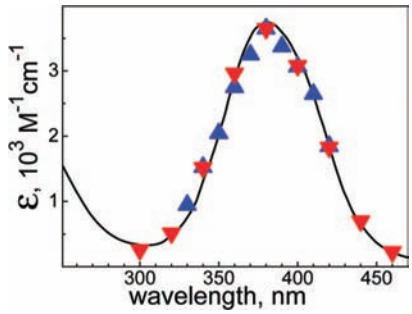

Figure 5. Absorption spectra of the $N_3O_3^-$ transient obtained through NO reduction with e_{aq}^- (reaction 13, solid line),[4] from the absorption maxima on the transient kinetics (Figure 6) for a N_2O-saturated solution of $N_2O_2^{2-}$ using eq 14 (blue up triangles), and from the initial absorption (Figure 6) for a $N_2O_2^{2-}$ solution saturated with a 99:1 N_2O/NO mixture (reactions 10 and 11, red down triangles).

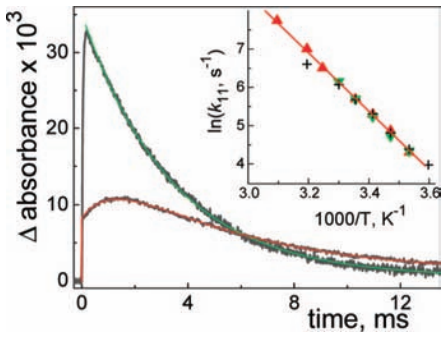

Figure 6. Typical kinetic traces recorded at 380 nm following pulse radiolysis (dose of 2.8 Gy or 0.29 μM of radicals per unit G value) of a 1.3 mM $Na_2N_2O_2$ alkaline (66 mM NaOH, μ = 70 mM) solution. Lower trace: N_2O-saturated solution. The red line shows the numerical integration fit to reactions 6′ and 11 with $2k_{6'} = 2.7 \times 10^8$ M^{-1} s^{-1} and $k_{11} = 3.3 \times 10^2$ s^{-1}; essentially the same fit (indistinguishable without magnification) is produced by using reactions 6a, 10, and 11 with $2k_{6a} = 1.4 \times 10^8$ M^{-1} s^{-1}, $k_{10} = 5.4 \times 10^9$ M^{-1} s^{-1}, and $k_{11} = 3.3 \times 10^2$ s^{-1}. Upper trace: solution saturated with a 99:1 N_2O/NO mixture (19 μM of dissolved NO). The green line gives a first-order decay fit with a 3.0×10^2 s^{-1} rate constant. The inset shows Arrhenius dependence for the decay at 380 nm observed above pH 7 in a NO-saturated solution with no added $Na_2N_2O_2$ (red up triangles), a 2 mM $Na_2N_2O_2$ solution saturated with a 99:1 N_2O/NO mixture (green down triangles), and a N_2O-saturated 2 mM $Na_2N_2O_2$ solution (crosses). The straight line gives activation energy E_a = 15.2 kcal/mol and pre-exponential factor $A = 3.9 \times 10^{13}$ s^{-1}.

reaction has an absorption maximum at 380 nm (Figure 5) and decays on the millisecond time scale (Figure 6).

Analysis of Scheme 1A can be simplified by recognizing that reaction 10 (previously estimated $k_{10} = 5.4 \times 10^9$ M^{-1} s^{-1})[4] is much more rapid than reaction 6a under the prevailing conditions and by replacing reactions 6a and 10 with a single bimolecular reaction; that is, reaction 6 can be reformulated as

$$N_2O_2^{\bullet-} + N_2O_2^{\bullet-} \rightarrow 0.5N_2O_2^{2-} + N_3O_3^- \qquad (6')$$

Considering stoichiometry, the apparent rate constant for this reaction is related to the rate constant of reaction 6a as $k_{6'} \approx 2k_{6a}$. The validity of this approach is illustrated in Figure 6 with the help of numerical simulations. Although the kinetics due to reactions 6′ and 11 can be integrated, the result—an infinite series—is not particularly useful. However, a simple expression for determining the molar absorptivity of $N_3O_3^-$ from the amplitude (A_{max}) and time (t_{max}) of the kinetic absorption maximum (like the one appearing in Figure 6, lower trace) can be derived

$$\frac{\varepsilon(N_3O_3^-)}{2} = \frac{A_{max}}{[N_2O_2^{\bullet-}]_0} \times \frac{(\tau_{6'} + t_{max})^2}{\tau_{6'}\tau_{11}} + \varepsilon(N_2O_2^{\bullet-})\frac{\tau_{11} - \tau_{6'} - t_{max}}{\tau_{11}} \qquad (14)$$

where $[N_2O_2^{\bullet-}]_0$ and $\varepsilon(N_2O_2^{\bullet-})$ are the initial concentration and molar absorptivity for the hyponitrite radical and $\tau_{6'} = 1/(2k_{6'}[N_2O_2^{\bullet-}]_0)$ and $\tau_{11} = 1/k_{11}$ are the characteristic times of reactions 6′ and 11, respectively. This equation reflects the fact that $N_3O_3^-$ and $N_2O_2^{\bullet-}$ are the only species in the system absorbing between 330 and 420 nm where the maxima are observed in the transient kinetics. Application of eq 14 to these kinetics with the previously determined $N_2O_2^{\bullet-}$ spectrum[1] and $N_3O_3^-$ lifetime (3.3 ms)[4] and with the values for $[N_2O_2^{\bullet-}]_0$ and $\tau_{6'}$ independently measured at 290 nm at the prevailing ionic strength yields a spectrum that closely matches "authentic" $N_3O_3^-$ (Figure 5).

The same spectrum was obtained when a small amount of NO was added to the solution of $N_2O_2^{2-}$ prior to irradiation (Figure 5). This was done by bubbling a mixture of N_2O and NO (99:1), which yields a solution 19 μM in NO. This concentration is too low for NO to compete with N_2O for the hydrated electron or with $N_2O_2^{2-}$ for the $OH^\bullet$ radical,[1,4] but it is sufficient to efficiently compete with recombination of $N_2O_2^{\bullet-}$, assuring complete scavenging of this radical via reaction 10. As shown in Figure 6, the 380 nm intermediate absorbance appears promptly after the pulse, and its amplitude more than doubles that obtained in the absence of NO because now every $N_2O_2^{\bullet-}$ is intercepted through reaction 10. The intermediate decay is purely first-order. The rate of this decay and the spectrum of initial absorbance identify the intermediate as $N_3O_3^-$.

Additional evidence for this assignment comes from the temperature dependence for the intermediate decay rate (Figure 6, inset). The decay of $N_3O_3^-$ obtained through reaction sequence 13 in the NO-saturated solution is strongly activated; we obtain $E_a = 15.2 \pm 0.2$ kcal/mol and $A = (2.8-5.6) \times 10^{13}$ s^{-1} for the Arrhenius parameters. This activation energy is in excellent agreement with the previously reported value,[3] and the pre-exponential factor is consistent with a simple bond breaking. Essentially the same activation is observed for the 380 nm intermediate produced from the $N_2O_2^{\bullet-}$ radical either through reactions 6a and 10 in the absence of added NO or by reaction 10 only in the presence of small amounts of added NO (Figure 6, inset).

An alternative recombination mechanism kinetically indistinguishable from that in Scheme 1A and yielding the same overall stoichiometry (reaction 12) can be envisioned, in which $N_3O_3^-$ is formed directly by the NO group transfer

$$N_2O_2^{\bullet-} + N_2O_2^{\bullet-} \rightarrow {}^3NO^- + N_3O_3^- \qquad (6b)$$

followed by the coupling of two $^3NO^-$ to regenerate $N_2O_2^{2-}$

$$^3NO^- + {}^3NO^- \rightarrow N_2O_2^{2-} \qquad (15)$$

and by the decay of $N_3O_3^-$ via reaction 11. This scenario is shown in Scheme 1B, and the principal difference between this and the mechanism starting with reaction 6a is in the intermediacy of $^3NO^-$ instead of NO. To distinguish between these two cases, experiments were performed in the presence of dissolved oxygen, and the formation of peroxynitrite ($ONOO^-$) exhibiting a characteristic UV spectrum (λ_{max} = 302 nm, ε = 1670 M^{-1} cm^{-1})[22] has been examined.

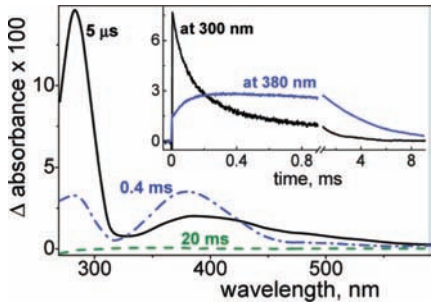

Figure 7. Transient absorption spectra measured at 5 μs ($N_2O_2^{\bullet-}$ radical, solid black), 0.4 ms (mainly $N_3O_3^-$, dash−dot blue), and 20 ms (dash green) after laser flash photolysis of an O_2-saturated solution containing 50 mM persulfate and 6.6 mM hyponitrite at pH 9.2 (10 mM Borax). The inset shows kinetics at 300 ($N_2O_2^{\bullet-}$ decay, black) and 380 nm ($N_3O_3^-$ formation and decay, blue); note the time axis break.

Should reaction 6b occur, its $^3NO^-$ product would rapidly combine with O_2 to quantitatively yield peroxynitrite in the oxygen-saturated (1.3 mM in O_2) solutions[5]

$$^3NO^- + O_2 \rightarrow ONOO^- \qquad k_{16} = 2.7 \times 10^9\ M^{-1}\ s^{-1} \tag{16}$$

This possibility was investigated with a previously described method of generating the $N_2O_2^{\bullet-}$ radical by laser flash photolysis,[1] in which the photochemical cleavage of persulfate yields the $SO_4^{\bullet-}$ radicals that rapidly oxidize hyponitrite

$$S_2O_8^{2-}(+h\nu) \rightarrow 2SO_4^{\bullet-} \qquad \lambda = 308\ nm \tag{17}$$

$$HN_2O_2^- + SO_4^{\bullet-} \rightarrow N_2O_2^{\bullet-} + SO_4^{2-} + H^+ \qquad k_{18} = 6.4 \times 10^8\ M^{-1}\ s^{-1} \tag{18}$$

The results shown in Figure 7 clearly demonstrate that no peroxynitrite formation is observed at around 300 nm upon the decay of all transients. Thus, reactions 6b and 16 do not occur; that is, Scheme 1B does not represent the actual mechanism. Figure 7 also shows that decay of the UV band of $N_2O_2^{\bullet-}$ is accompanied by formation of the 380 nm absorption due to $N_3O_3^-$; the $N_2O_2^{\bullet-}$ decay follows second-order kinetics.

The validity of Scheme 1A has been examined by pulse radiolysis of the hyponitrite solutions saturated either with pure O_2 or with a 9:1 N_2O to O_2 gaseous mixture. In both cases, essentially all radiolytically generated H atoms are scavenged by O_2 to produce superoxide ($O_2^{\bullet-}$), but the solvated electrons generate $O_2^{\bullet-}$ only in the O_2-saturated solution; in the N_2O/O_2 mixture, almost 99% of e_{aq}^- is converted into $OH^\bullet$ by reaction with N_2O.[23] If reaction 6a takes place and NO is released, peroxynitrite can be produced by combination with superoxide[24]

$$NO + O_2^{\bullet-} \rightarrow ONOO^- \qquad k_{19} = 4.8 \times 10^9\ M^{-1}\ s^{-1} \tag{19}$$

and peroxynitrite formation should be much more extensive under oxygen saturation. This follows because the radiation yields of a limiting reactant in reaction 19 are 2.8 (NO) and 0.6 ($O_2^{\bullet-}$) for solutions saturated with O_2 and N_2O/O_2, respectively.

This is indeed the case, as shown by the magnitudes and the spectra of the persisting residual absorption in Figure 8, left panel, which belongs to peroxynitrite. This assignment is corroborated by the rate of the residual absorption decay and its pH dependence (Figure 8, right panel), which are both characteristic of peroxynitrite; the pH dependence reflects the known pK_a of ONOOH and the fact that the acid form, whose characteristic lifetime is about 1 s, is solely responsible for the overall peroxynitrite decay at around neutral pH.[25] The formation kinetics and magnitudes of residual absorption plateaus at 30−50 ms in Figure 8 can be reproduced by numerical simulations using reactions 6a, 10, 11, and 19 for both O_2-containing solutions (for the simulated fits, see Supporting Information Figure S2). The computed peroxynitrite yields (expressed as the $[ONOO^-]_{t=50ms}/[N_2O_2^{\bullet-}]_{t=0}$ ratio) are 51 and 8% for solutions saturated with O_2 and N_2O/O_2, respectively. The yield close to 50% in the former case arises because the rate constants for reactions 10 and 19 are about the same and the initial concentrations of $N_2O_2^{\bullet-}$ and $O_2^{\bullet-}$ are also comparable. The near 10% yield for the latter case simply reflects the $[O_2^{\bullet-}]_{t=0}/[N_2O_2^{\bullet-}]_{t=0} = 0.6/6.1$ ratio of initial concentrations. We thus conclude that the pattern of peroxynitrite formation is fully consistent with the mechanism shown in Scheme 1A plus reaction 19.

An assumption implicit in this analysis is the absence of interference from direct reactions between the $N_2O_2^{\bullet-}$ radical and either O_2 or $O_2^{\bullet-}$, for example, the electron transfers

$$N_2O_2^{\bullet-} + O_2 \rightarrow 2NO + O_2^{\bullet-} \tag{20}$$

$$N_2O_2^{\bullet-} + O_2^{\bullet-} \rightarrow N_2O_2^{2-} + O_2 \tag{21}$$

A comparison of the $N_2O_2^{\bullet-}$ decay kinetics in Figure 9 shows that this is indeed the case. Because the decay reaction is second-order in character, radiation doses have been applied such that very nearly equal amounts of $N_2O_2^{\bullet-}$ are generated in all N_2O-saturated, N_2O/O_2-saturated, and O_2-saturated solutions. It is seen that the kinetics are practically indistinguishable in the first two cases, indicating that O_2 does not appreciably react with $N_2O_2^{\bullet-}$. For the O_2-saturated solutions, where large amounts of $O_2^{\bullet-}$ are also produced, the $N_2O_2^{\bullet-}$ decay appears even slower than that in the other two cases. However, this effect is only apparent and is explicable by the simultaneous formation of $ONOO^-$ and by the excess of unreacted $O_2^{\bullet-}$, whose absorptions overlap with that of $N_2O_2^{\bullet-}$. In fact, this explanation is born out by the kinetic simulations, confirming the absence of interference from a direct reaction between $O_2^{\bullet-}$ and $N_2O_2^{\bullet-}$ under our experimental conditions. Specifically, a good fit can be obtained using only reactions 6a, 10, 11, and 19; inclusion of reactions 20 and 21 seriously spoils the fit if their rate constants exceed 1×10^6 and $5 \times 10^7\ M^{-1}\ s^{-1}$, respectively.

Discussion

Collectively, all of the data presented are consistent with the disproportionation mechanism that involves a short chain (Scheme 1A), where the rate-determining step is reaction 6a producing NO as an intermediate. Applying our previous estimates for the reduction potentials $E^o(N_2O_2^{\bullet-}/N_2O_2^{2-}) = 0.96$ and $E^o(2NO/N_2O_2^{\bullet-}) = -0.38$ V versus NHE,[1] we calculate that this reaction is exergonic by 1.34 eV. In contrast, recently published potentials $E^o(N_2O_2^{\bullet-}/N_2O_2^{2-}) = -0.4$ and $E^o(2NO/N_2O_2^{\bullet-}) = -0.1$ V based on ab initio calculations[26,27] predict that reaction 6a is endergonic by 0.3 eV, which appears to be inconsistent with the fairly high reaction rate. We will thus consider the energetics in detail.

Scheme 2 shows a thermodynamic cycle composed of acid−base and redox reactions of hyponitrite. It is clear that with our free-energy estimates, the cycle is closed within 0.01 eV; in contrast, the theoretically computed values leave the cycle open by 1.3 eV (30 kcal/mol). This number gives a cumulative error of computational results because the standard free-

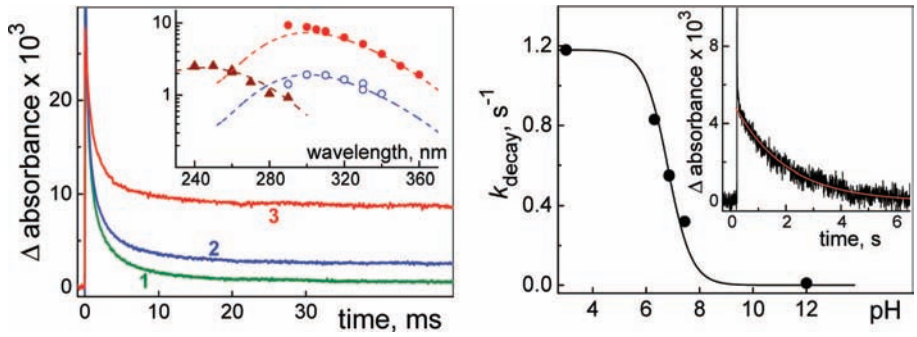

Figure 8. (Left panel) Kinetic traces recorded at 300 nm following pulse radiolysis (doses 26−28 Gy) of 4.8 mM $Na_2N_2O_2$ in 5 mM Borax (pH 9.2). Trace 1 (green): N_2O-saturated solution; trace 2 (blue): solution saturated with a 9:1 N_2O/O_2 mixture; trace 3 (red): O_2-saturated solution. The residual absorbances at around 50 ms correspond to approximately 10 and 50% peroxynitrite yields per $N_2O_2^{\bullet-}$ for the N_2O/O_2-saturated and O_2-saturated solutions, respectively. The inset compares the spectra of residual absorbances (solid symbols) with normalized spectra of authentic, chemically synthesized $ONOO^-$ (red and blue dashed lines) and ONOOH (brown dashed line). Circles: O_2-saturated alkaline solution. Squares: N_2O/O_2-saturated alkaline solution. Triangles: O_2-saturated acidic (pH 3) solution. All data are normalized to a 1 cm optical path. (Right panel) Dependence upon pH of the first-order rate constant for the decay of residual absorbance due to $ONOO^-$/ONOOH in the O_2-saturated 2 mM $Na_2N_2O_2$ solutions. The titration-like curve corresponds to $k_{decay} = k[H^+]/(K_a + [H^+])$ with $pK_a = 6.8$ and $k = 1.18\ s^{-1}$. The inset shows typical decay kinetics at 300 nm and pH 6.78 (phosphate) and its exponential fit (red line).

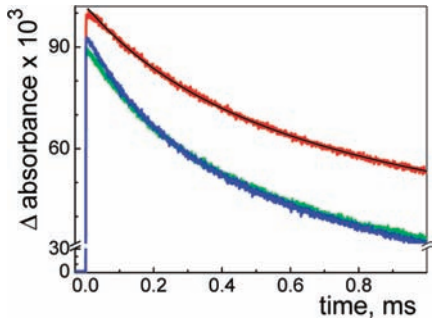

Figure 9. Comparison of the initial stages of the $N_2O_2^{\bullet-}$ radical decay as observed in a 2 cm cell at 290 nm following pulse radiolysis of 4.8 mM $Na_2N_2O_2$ in 5 mM Borax buffer (pH 9.2). Blue trace: N_2O-saturated solution (radiation dose 12.5 Gy). Green trace: solution saturated with a 4:1 N_2O/O_2 mixture (dose 12.7 Gy). Red trace: O_2-saturated solution (dose 25.6 Gy); the black line superimposed with this trace gives a numerical simulation fit that includes reactions 6a, 10, 11, and 19.

SCHEME 2: Thermochemical Cycle Involving Hyponitrite Species and Their Radicals in Aqueous Solution[a]

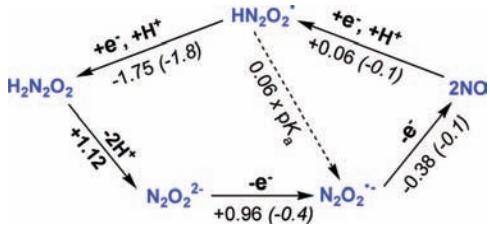

[a] The numbers correspond to free-energy changes (in eV/molecule, 1 M standard states, NHE reference) in the arrow directions. Entries in roman are our estimates;[1] italicized entries in parentheses are theoretical results by Houk and co-workers;[26,27] the number in bold is derived from the experimental pK_a values for hyponitrous acid.

energy change of 1.12 eV associated with full deprotonation of $H_2N_2O_2$ is set by the measured $pK_a(H_2N_2O_2) = 7.2$ and $pK_a(HN_2O_2^-) = 11.5$.[21]

The dashed diagonal arrow in Scheme 2 corresponds to deprotonation of the $HN_2O_2^{\bullet}$ radical, and its $pK_a = 5.6$ derived from the data in Figure 4 is consistent with our free-energy data. With the computed values[26,28] however, this pK_a depends on which side of the cycle is used and comes out as either 3.3 or −18 for the right and left side, respectively. The −18 number is particularly troublesome for it would make $HN_2O_2^{\bullet}$ a

SCHEME 3: Possible Pathways for the $N_2O_2^{\bullet-} + N_2O_2^{\bullet-}$ Reaction

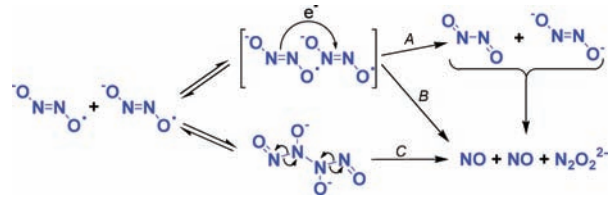

superacid for no apparent reason. From this analysis, the largest error in the theoretically derived energetics is clearly associated with the step of oxidizing $N_2O_2^{2-}$ to $N_2O_2^{\bullet-}$. On the basis of the electrostatics and electronic structure considerations, Houk and co-workers argued that their computed numbers[26] are more reasonable then our results specifically for this step. In our view, the failure of the ab initio calculations in the thermodynamic cycle test, primarily due to the $N_2O_2^{2-}$-to-$N_2O_2^{\bullet-}$ step, makes arguing at the electronic structure level moot and leaves our prior estimates as the only self-consistent data set.

It is perhaps not surprising that despite a very large driving force, reaction 6a between two radicals occurs with a rate that is some 2 orders of magnitude below the diffusion control because the reaction involves bond(s) breaking and, possibly, making. Probable mechanisms for this reaction are shown in Scheme 3, where pathways A and B represent intermolecular electron transfer occurring in a collision complex. In the adiabatic pathway B, an electron is transferred simultaneously with the N−N bond breaking, which would require large nuclear reorganization. For pathway A, a significant nuclear reorganization energy is also expected due to drastic differences between the N−N bond lengths and N−N−O angles in reactants and products (2.26 Å and 97°, 1.36−1.40 Å and 111°, and 1.26 Å and 112° for N_2O_2, $N_2O_2^{\bullet-}$, and $N_2O_2^{2-}$, respectively[16,17,29,30]). In addition, the nascent oxidized product for this pathway, *trans*-N_2O_2 dimer, is unstable with respect to two separated NO; in the gas phase, the free-energy difference is 0.6−0.8 eV,[28,31−33] which makes pathway A less exoergic than pathway B. The third possibility does not involve electron transfer at all and could occur via a radical dimerization, followed by homolytic eliminations of the NO end groups (case C). However, our data give no evidence, either spectral or kinetic, for an intermediate, so that if the reaction does occur through pathway C, the steady-state concentration of the $N_4O_4^{2-}$ intermediate has to be small

due either to its short lifetime or low equilibrium constant for its formation, or both. The absence of oxygen interference with the $N_2O_2^{\bullet-}$ decay on a millisecond time scale, evident in Figure 9, implies that reactions 20 and 21 are slow despite their considerable driving force; we estimate $\Delta_{r20}G^o \approx -5$ kcal/mol and $\Delta_{r21}G^o \approx -26$ kcal/mol. The assumption of large nuclear reorganization barriers for both reduction and oxidation of $N_2O_2^{\bullet-}$ would be in qualitative accord with their low rates. In view of this discussion, we are inclined to favor the radical recombination pathway C in Scheme 3.

It has been suggested that the hyponitrite radical is unstable toward unimolecular decomposition

$$ONNO^{\bullet-} \rightarrow N_2O + O^{\bullet-} \quad (22)$$

with the rate constant $k_{22} = 350\ s^{-1}$.[3] Thermodynamically, this reaction is reasonable; we calculate it to be downhill by 8 kcal/mol in free energy. However, our kinetic data on the $N_2O_2^{\bullet-}$ decay show no first-order component of this magnitude in the essentially pure second-order process, as evidenced by a negligible intercept in the upper panel of Figure 2. Moreover, the occurrence of reaction 22 would regenerate $OH^{\bullet}$ ($pK_a \approx 12$),[34,35] triggering a chain decomposition of hyponitrite. This effect should be especially prominent under continuous, low-intensity radiation when the self-recombination pathways for $N_2O_2^{\bullet-}$ are minimized. And yet, our gamma radiolysis experiment gives a hyponitrite decomposition radiation yield that is below the yield for $OH^{\bullet}$ and is in accord with the stoichiometry of reaction 12 (Supporting Information Figure S1). Thus, reaction 22 does not occur with a detectable rate. The most apparent reason for this is that the reaction is not merely dissociation along the N−O bond; a very large nuclear reorganization is required to form a linear N_2O product from a nonlinear reactant. An instructive analogy here is the unimolecular dissociation of monoprotonated hyponitrite anion, $HONNO^-$, to yield N_2O and OH^-. Although more exergonic ($\Delta G^o \approx -30$ kcal/mol) than reaction 22, this decomposition occurs with a 16 min half-life.[1,36] Reaction 22 is probably even slower, and it appears that previous speculations concerning the role of $N_2O_2^{\bullet-}$ as a OH-releasing species in biological environments[37,38] should be reconsidered.

The data for the solution without deliberately added NO in Figures 5 and 6 can be used for estimating the upper limit of reversibility in reaction 10. Specifically, simulations show that it is not possible to maintain the molar absorptivity of $N_3O_3^-$ at 380 nm within 10% of its nominal value and obtain even remotely satisfactory fits to the absorption kinetics at this wavelength if the rate constant for decomposition of $N_3O_3^-$ back to $N_2O_2^{\bullet-}$ and NO exceeds some 3000 s^{-1}. Thus, the dissociation constant K_{-10} does not exceed 5×10^{-7} M (a rather conservative upper limit), in agreement with our previous estimate,[4] and the free energy of formation, $\Delta_f G^o$, for aqueous $N_3O_3^-$ is below 73 kcal/mol. On the other hand, the occurrence of spontaneous $N_3O_3^-$ decomposition via reaction 11 sets the lower limit for $\Delta_f G^o$, so that $18 < \Delta_f G^o(N_3O_3^-) < 73$ kcal/mol.

Most of the data presented above pertain to the deprotonated hyponitrite radical, primarily because information on the recombination mechanism that could be obtained for the radical's conjugate acid ($HN_2O_2^{\bullet}$) predominating below pH 5 is more limited. In the acidic pH region, considerable experimental difficulties arise from drastic decreases in both the absorption and lifetime of the $N_3O_3^-$ intermediate, undoubtedly due to formation of the HN_3O_3 species. These effects have been reported previously, and the rate constant of $k_{23} = 1.6 \times 10^4\ s^{-1}$ for the dissociation

$$HN_3O_3 \rightarrow N_2O + HNO_2 \quad (23)$$

has been reported along with a pK_a of 3.1 for HN_3O_3.[2,3] Our observations are in general agreement with these results. Despite the increased rate of the $HN_2O_2^{\bullet}$ recombination (Figure 4), we no longer observe the formation kinetics for $HN_3O_3/N_3O_3^-$; only vestiges of their decay can be detected (Figure 2, upper panel). The decay rate sharply increases below pH 4 in a manner consistent with the reported pK_a and k_{23} (Supporting Information Figure S3). However, we do observe formation of peroxynitrous acid, ONOOH, in the quantitatively correct amounts when oxygen is present and superoxide is generated (Figure 8, left panel inset), which implies the intermediacy of NO. On the basis of this fact, we believe that the recombination of $HN_2O_2^{\bullet}$ occurs by a mechanism analogous to that shown in Scheme 1A, that is, the rate-limiting radical disproportionation

$$HN_2O_2^{\bullet} + HN_2O_2^{\bullet} \rightarrow H_2N_2O_2 + 2NO \quad (7a)$$

is followed by a rapid combination reaction

$$HN_2O_2^{\bullet} + NO \rightarrow HN_3O_3 \quad (24)$$

and finally by the HN_3O_3 decay in reaction 23. If $k_{24} \gg k_{7a}$, the rate constant k_{7a} is 1/4 of the slope in the lower panel in Figure 3, or $k_{7a} = 5.5 \times 10^8\ M^{-1}\ s^{-1}$.

Acknowledgment. Research at Brookhaven National Laboratory was carried out under the auspices of the U.S. Department of Energy under Contract DE-AC02-98CH10886 from the Division of Chemical Sciences, Office of Basic Energy Sciences. Helpful comments from Drs. Norman Sutin and Harold Schwarz are appreciated.

Supporting Information Available: Details of kinetic simulations (tabulated rate constants, spectral properties, and radiation yields); gamma radiolysis results; expanded view of kinetic fits for Figure 8; and pH dependence of $HN_3O_3/N_3O_3^-$ decay. This material is available free of charge via the Internet at http://pubs.acs.org.

References and Notes

(1) Poskrebyshev, G. A.; Shafirovich, V.; Lymar, S. V. *J. Am. Chem. Soc.* **2004**, *126*, 891.
(2) Grätzel, M.; Taniguchi, S.; Henglein, A. *Ber. Bunsen-Ges. Phys. Chem.* **1970**, *74*, 1003.
(3) Seddon, W. A.; Fletcher, J. W.; Sopchyshyn, F. C. *Can. J. Chem.* **1973**, *51*, 1123.
(4) Lymar, S. V.; Shafirovich, V.; Poskrebyshev, G. A. *Inorg. Chem.* **2005**, *44*, 5212.
(5) Shafirovich, V.; Lymar, S. V. *Proc. Natl. Acad. Sci. U.S.A.* **2002**, *99*, 7340.
(6) Shafirovich, V.; Lymar, S. V. *J. Am. Chem. Soc.* **2003**, *125*, 6547.
(7) Lymar, S. V.; Shafirovich, V. *J. Phys. Chem. B* **2007**, *111*, 6861.
(8) Posey, L. A.; Johnson, M. A. *J. Chem. Phys.* **1988**, *88*, 5383.
(9) Li, R.; Continetti, R. E. *J. Phys. Chem. A* **2002**, *106*, 1183.
(10) Jacox, M. E.; Thompson, W. E. *J. Chem. Phys.* **1990**, *93*, 7609.
(11) Andrews, L.; Zhou, M. F.; Willson, S. P.; Kushto, G. P.; Snis, A.; Panas, I. *J. Chem. Phys.* **1998**, *109*, 177.
(12) Andrews, L.; Zhou, M. F. *J. Chem. Phys.* **1999**, *111*, 6036.
(13) Lugez, C. L.; Thompson, W. E.; Jacox, M. E.; Snis, A.; Panas, I. *J. Chem. Phys.* **1999**, *110*, 10345.
(14) Mebel, A. M.; Morokuma, K.; Lin, M. C.; Melius, C. F. *J. Phys. Chem.* **1995**, *99*, 1900.
(15) Bunte, S. W.; Rice, B. M.; Chabalowski, C. F. *J. Phys. Chem. A* **1997**, *101*, 9430.
(16) Snis, A.; Panas, I. *Chem. Phys.* **1997**, *221*, 1.
(17) Fuster, F.; Dezarnaud-Dandine, C.; Chevreau, H.; Sevin, A. *Phys. Chem. Chem. Phys.* **2004**, *6*, 3228.
(18) Polydoropoulos, C. N.; Voliotis, S. D. *Anal. Chim. Acta* **1968**, *40*, 170.

(19) The Numerical Integration method used in this program is the DVODE package written by P. N. Brown and A. C. Hindmarsh of Lawrence Livermore National Laboratory, and G. D. Byrne of Exxon Research and Engineering Co.

(20) In alkaline solutions, these reactions are $H + OH^- \rightarrow e_{aq}^- + H_2O$ and $e_{aq}^- + N_2O + H_2O \rightarrow N_2 + OH^- + OH$. In acidic solutions, the following reactions occur: $e_{aq}^- + H^+ \rightarrow H$ and $H_2N_2O_2 + H \rightarrow H_2O + N_2 + OH$. For detail, see: Poskrebyshev, G. A.; Lymar, V. *J. Am. Chem. Soc.* **2004**, *126*, 891.

(21) Bonner, F. T.; Hughes, M. N. *Comments Inorg. Chem.* **1988**, *7*, 215.

(22) Hughes, M. N.; Nicklin, H. G. *J. Chem. Soc. A* **1968**, 450.

(23) Buxton, G. V.; Greenstock, C. L.; Helman, W. P.; Ross, A. B. *J. Phys. Chem. Ref. Data* **1988**, *17*, 513.

(24) Lymar, S. V.; Poskrebyshev, G. A. *J. Phys. Chem. A* **2003**, *107*, 7991.

(25) Goldstein, S.; Lind, J.; Merenyi, G. *Chem. Rev.* **2005**, *105*, 2457.

(26) Dutton, A. S.; Fukuto, J. M.; Houk, K. N. *Inorg. Chem.* **2005**, *44*, 4024.

(27) Dutton, A. S.; Fukuto, J. M.; Houk, K. N. *Inorg. Chem.* **2005**, *44*, 7687.

(28) Dutton, A. S.; Fukuto, J. M.; Houk, K. N. *Inorg. Chem.* **2004**, *43*, 1039.

(29) McKellar, A. R. W.; Watson, J. K. G.; Howard, B. J. *Mol. Phys.* **1995**, *86*, 273.

(30) Kukolich, S. G.; Sickafoose, S. M. *Mol. Phys.* **1996**, *89*, 1659.

(31) Dkhissi, A.; Soulard, P.; Perrin, A.; Lacome, N. *J. Mol. Spectrosc.* **1997**, *183*, 12.

(32) Urban, B.; Strobel, A.; Bondybey, V. E. *J. Chem. Phys.* **1999**, *111*, 8939.

(33) Park, J. K.; Sun, H. *Chem. Phys.* **2001**, *263*, 61.

(34) Hickel, B.; Corfitzen, H.; Sehested, K. *J. Phys. Chem.* **1996**, *100*, 17186.

(35) Poskrebyshev, G. A.; Neta, P.; Huie, R. E. *J. Phys. Chem. A* **2002**, *106*, 11488.

(36) Hughes, M. N.; Stedman, G. *J. Chem. Soc.* **1963**, 1239.

(37) Ohshima, H.; Gilibert, I.; Bianchini, F. *Free Radical Biol. Med.* **1999**, *26*, 1305.

(38) Kirsch, M.; de Groot, H. *J. Biol. Chem.* **2002**, *277*, 13379.

JP803230C